RSC Advances

ROYAL SOCIETY OF CHEMISTRY

www.rsc.org/advances

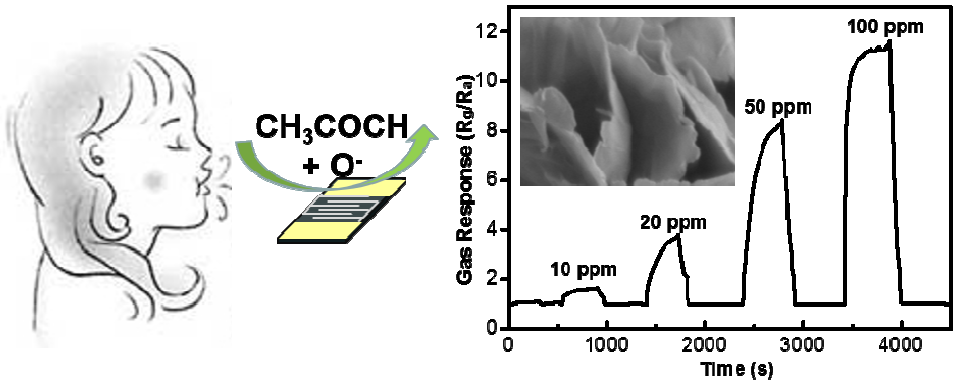

The gas sensors based on ultrathin porous Co_3O_4 nanosheets to detect acetone for diagnosing diabetes at low operating temperature.

Cite this: DOI: 10.1039/c0xx00000x

www.rsc.org/xxxxxx

ARTICLE TYPE

Gas sensor based on ultrathin porous Co_3O_4 nanosheets to detecting acetone at low temperature

Ziyue Zhang, Zhen Wen, Zhizhen Ye and Liping Zhu*

Received (in XXX, XXX) Xth XXXXXXXXX 20XX, Accepted Xth XXXXXXXXX 20XX

DOI: 10.1039/b000000x

By a facile two-step process, including a hydrothermal technique and subsequently controlled annealing of the precursor, ultrathin porous Co_3O_4 nanosheets can be synthesized. The gas sensor based on the porous Co_3O_4 nanosheets shows superior acetone gas-sensing performances at a low operating temperature of 150°C. The gas response to 100ppm acetone reached 11.4, and exhibited good reproducibility. In addition, the detection limit of the Co_3O_4 nanosheets sensor is lower than 1.8 ppm, which is the diagnostic criteria exhaled from diabetes. What's more, the sensor exhibited good stability tested in 2 months. The outstanding gas-sensing properties were explained by a typical *p*-type behavior with ultrathin porosity structure as well as large specific surface area of Co_3O_4 nanosheets.

Introduction

With the increasingly prominent issue concerning food and environment, people are paying much more emphasis on the advanced diagnosis of their health conditions. The regular physical examination, consists of ultrasonication, electrocardio and irradiation as well as testing blood and urine,[1] are time and resource consuming and inconvenient. During the past few years, a testing approach utilizing the analysis of the exhaled breath from human bodies to make an initial judgment of the physical condition has been proposed by researchers.[2] Basically, the exhaled breath of healthy people contains carbon dioxide, nitrogen, vapour, rare gases and various organic gases produced in the metabolic process.[3, 4] If a certain gas concentration is beyond a normal range, it almost means that the human is ill.[5] For instance, diabetes, asthma, heart disease, kidney malfunction and chronic obstructive pulmonary disease are closely relate to the concentration of exhaled acetone, nitrogen monoxide, pentane, ammonia, carbon monoxide, respectively.[6] Among these illness, diabetes is the most common chronic disease at present. If it can found at early stage, the people with pre-diabetes can sharply lower their chances of developing the disease.[7, 8] Nowadays, gas chromatographic detection technology, selected ion flow tube mass spectrometry and cavity ring down spectroscopy are the most common diagnostic techniques to detect the acetone in exhaled breath.[9-12] But, in addition to these detection technology, gas sensors have great potential to be used as acetone testing instrument in the future, due to its advantages, such as, small, portable and low-cost.

Due to the inherent advantages of gas sensors, such as portable, cheap and suitable for daily use.[13-16] People have begun to consider using gas sensor in detecting exhaled breath.[17, 18] For example, Marco Righettoni *et al.* developed the gas sensors based on Si-doped WO_3 to analysis breath acetone for diabetes detection at 400°C,[19] Li *et al.* synthesised Co-doped ZnO nanofibers-based gas sensors to detect acetone at 360°C,[20] Song *et al.* produced Ce doped SnO_2 hollow spheres as an acetone gas sensors at 250°C,[21] and Zhou *et al.* developed acetone gas sensors based on porous $ZnO/ZnCo_2O_4$ hollow spheres at 275°C.[22] However, in order to achieve their optimal sensing performances, these sensors usually have low sensitivity and ask for higher working temperatures, which not only shortens sensor lifetime but also increases the cost of practical applications. Thus, the large-scale application of these sensors in our daily life to detect diabetes is limited. In our previous work, we have reported the Co_3O_4 nanorod array-based ethanol gas sensor with low operating temperature.[23-25] Therefore, we try to prepare of a kind of Co_3O_4 to detect acetone for diagnosing diabetes at low operating temperature.

In this work, we present the fabrication of the ultrathin porous Co_3O_4 nanosheets-based gas sensor with high-performance for acetone selectively detection at relatively low temperature. The characterizations of the Co_3O_4 nanosheets consist of scanning electron microscopies (SEM), thermogravimetric analysis (TGA), X-ray diffraction (XRD), transmission electron microscopy (TEM), high-resolution TEM (HRTEM), Brunauer–Emmet–Teller (BET). Subsequently, the high-performance sensing properties of the gas sensor based on ultrathin porous Co_3O_4 nanosheets for acetone and the related gas-sensing mechanism will also be discussed.

Experimental

Co_3O_4 Nanomaterial Synthesis

All chemicals were of analytical grade and used as purchased without further purification. The typical experiments were as follow: Firstly, 0.02 mmol (0.125 g) Poly (ethylene glycol)-block-poly (propylene glycol)-block-poly (ethylene glycol) were dissolved in the mixing solution with 16.5 mL ethanol and 1 mL

high purity water (18.3 MΩ • cm resistivity) under stirring at room temperature. Secondly, after getting clarifying solution, put 0.5 mmol (0.07 g) Hexamethylenetetramine and 0.5 mmol (0.125 g) cobalt acetate ($C_4H_6O_4$•Co•$4H_2O$) into it and stirred at 60°C, then added 13 ml Ethylene glycol, until its colour changed from transparency to purity pink. Thirdly, the precursor solution were statically aged for 12 h. Fourthly, the homogeneous solution was transferred into a 50 ml Teflon-lined stainless steel autoclave, which was sealed and maintained at 170°C for 2 h inside an electric oven. Fifthly, after cooling down to room temperature spontaneously, the brown muddy solution in autoclave was washed with distilled water and ethanol several times, in order to remove the free nanoparticle debris and the residual reactant. The light green powders were collected through washing/centrifugation (10000 rpp, 3 min) and dried under vacuum at 60°C for 12 h. Finally, a series of Co_3O_4 nanosheets were fabricated by annealing the as-prepared light green powers at 250°C, 300°C, 350°C, 400°C and 450°C in air for 2 h, respectively (corresponding products denoted as S250, S300, S350, S400 and S450, respectively).

Characterization

The microstructures and morphologies of both the sample before annealing and the calcined products were examined using SEM (Hitachi, S-4800) with an accelerating voltage of 5 kV. The crystal phase identification were investigated by XRD (Bede D1) system with Cu-$K_{\alpha1}$ radiation (λ= 0.15406 nm) over the 2θ range of 10–70°. TEM and HRTEM images were taken by a HRTEM analyser with an accelerating voltage of 200 KV. TGA (SDT Q600) was carried out under the air atmosphere at 10°C/min in the temperature range 10-900°C. Specific surface areas were computed from the results of N_2 adsorption–desorption isotherms at 77 K (Micromeritics ASAP 3020).

Gas sensor Fabrication

The as-prepared powders were mixed with chitosan solution in the proper weight ratio to get 0.2 wt% CHIT solution and ground in a mortar over time to form a paste. The paste was coated on a

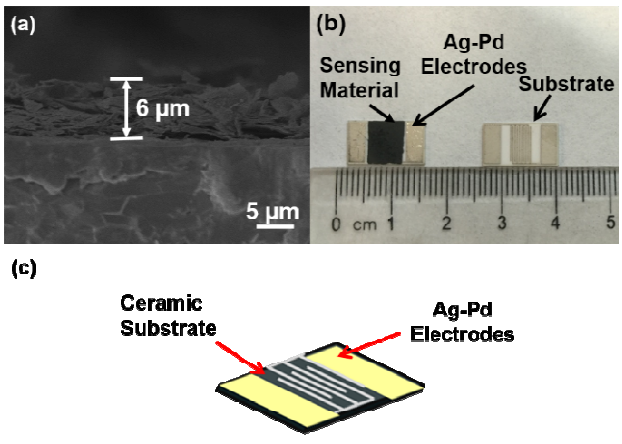

Fig.1 (a) SEM image of the section of sensor; (b) Top view of sensor substrate and sample sensors; (c) Schematic structure of sensor.

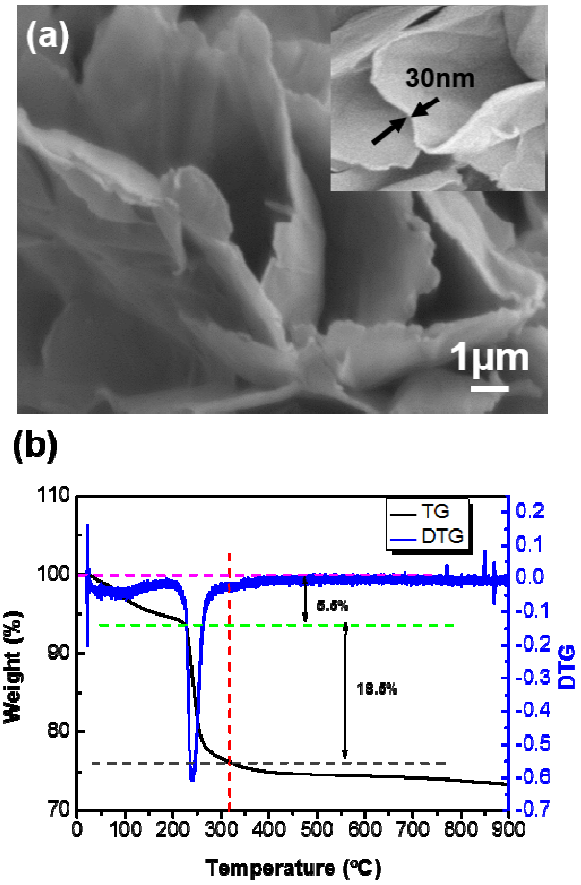

Fig. 2 Morphological and structural characterization of the precursor: (a) SEM image of Co_3O_4 nanosheets; (b) TGA/DTG curves under air with a ramp of 10°C·min^{-1}.

polycrystalline alumina ceramic plate (8 mm × 4 mm, 0.5 mm in thick) which had been plated with Ag-Pd finger regions (five pairs, both the width and distance are 200 mm) as electrodes to form a sensing film (with a thickness of ~6 μm, as shown in Fig. 1 (a)). Finally, annealed the samples at 60°C for 12 h. The top view of the sample sensor is shown in Fig. 1 (b). And Fig.1 (c) shows the schematic structure of sensor.

Gas-sensing Measurement

The detailed gas-sensing experiment process can be found in our previous report.[26] We measured the gas sensing properties of samples by an intelligent gas sensing analysis system (CGS-1TP, Beijing Elite Tech Co., Ltd, China). Two probes were pressed onto the sensor electrodes through adjusting the position in the analysis system. There is an external temperature control (from room temperature to 500°C), which could conductively adjust the sensor temperature with a precision of 1°C. First of all, the sensor was preheated at different operating temperatures for about 1 h to get the stable resistances. Then through a rubber plug, target gas was injected into the test chamber (18 L in volume) by a micro-injector. Our target liquid, e.g. acetone, was injected into the evaporator to form acetone vapour. By two fans in the analysis system, the saturated target gas was mixed with air (relative humidity was about 50%). After the sensor resistance reached a new constant value, opening the test chamber to recover the sensor in air. The gas response was designated as Rg/Ra, where

Rg is the sensor resistance measured in the presence of the target gas and Ra in air. Response and recovery times were defined as the time needed for 90% of total resistance change (Rg-Ra) on exposure to gas and air, respectively.

Results and discussion

Materials Characterization

The morphology and structure of the precursor obtained by the hydrothermal method were firstly investigated systematically. Fig. 2 (a) indicates that the precursor is random shape nanosheets with smooth surface and extremely thin (~30 nm). Fig. 2 (b) shows the thermodecomposition behavior of the precursor, which implies that there exists three decomposition steps: the first one appears below 200°C, with a weight loss of about 5.5%. The lose weight is mainly due to the evaporated adsorbed water of the sample. The second turning point appears at 310°C, with a distinct weight loss of about 18.5% between 200°C and 310°C, which is ascribed to the decomposition of the precursors, leading to the release of CO_2 and H_2O. Numerous fractured porous structures are formed, during this stage, accompanying gas evolution and solid volume contraction. The third step appears after 310°C, with the primary small nanoparticles growing up into larger particles and the fractured porous structures decreasing gradually.

In order to find the most suitable annealing temperature for ideal ultrathin porous Co_3O_4 nanosheets-based gas sensors, the samples were annealed at different temperatures (from 250°C to 450°C). The XRD patterns of S250-S450 shown in the Fig. 3 (a) indicates that all of the samples are pure cubic Co_3O_4 phases. With the increasing of annealing temperature, the intensity of the diffraction peaks increased, meaning that the grain size increased. The mean crystallite sizes are estimated from the (311) peak with the Scherrer formula, the grain sizes from S250 to S450 are 4.9 nm, 6.4 nm, 9.1 nm, 19.4 nm and 28.9 nm, respectively. Fig. 3 (b)-(f) show the high-magnification SEM images of the ultrathin Co_3O_4 nanosheets obtained at different annealing temperatures. We can see that all of these samples are also random-shaped nanosheets, but comparing with samples before annealing, these products have porous surface. These pores on the surface were formed during the thermal treatment,

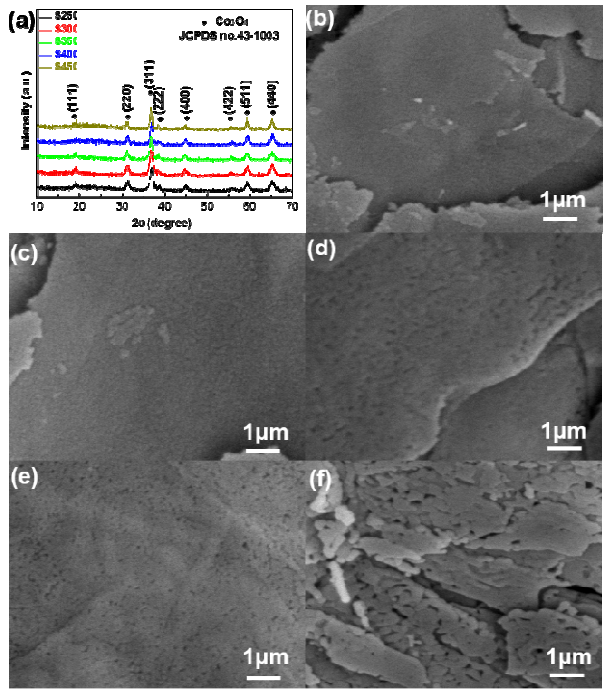

Fig. 3 (a) XRD patterns of S250~S450; (b)–(f) SEM images of Co_3O_4 nanosheets annealed at 250°C, 300°C, 350°C, 400°C and 450°C, respectively.

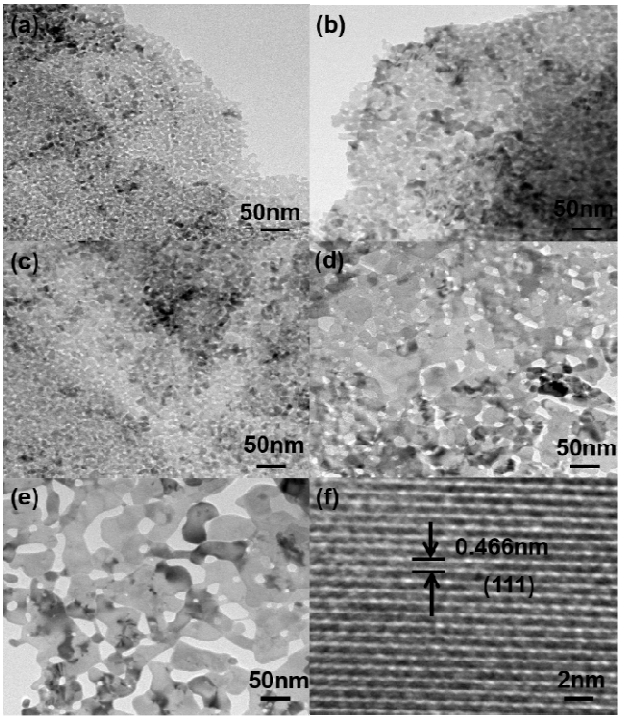

Fig. 4 TEM images of the porous Co_3O_4 nanosheets prepared at different annealing temperatures: (a) 250°C; (b) 300°C; (c) 350°C; (d) 400°C and (e) 450°C. (f) HRTEM image of the Co_3O_4 nanostructure annealed at 300°C.

because the generated CO_2 and H_2O (g) have out of samples. Comparing these SEM images, it can be found that both the size of nanoparticles and pores throughout the nanosheets are gradually increased, with the increasing annealing temperature.

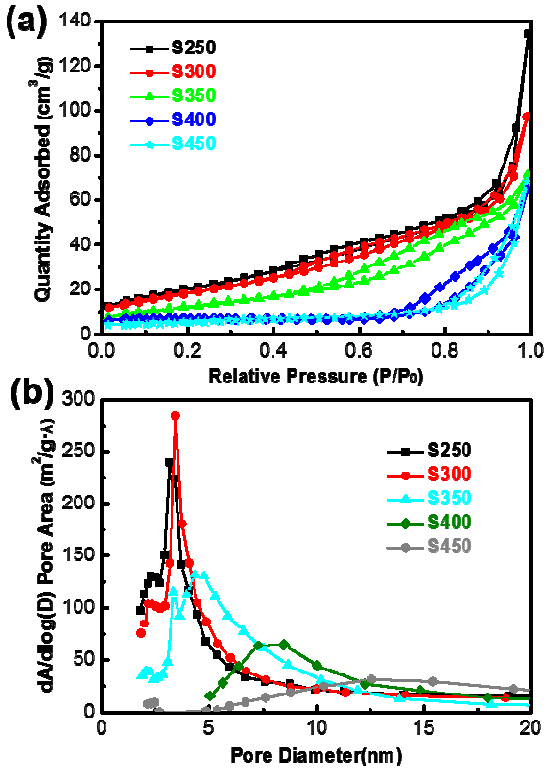

Fig. 5 (a) Nitrogen adsorption and desorption isotherms of the porous Co_3O_4 nanosheets with different annealing temperature; (b) Pore diameter distribution curves of the porous Co_3O_4 nanosheets with different annealing temperatures.

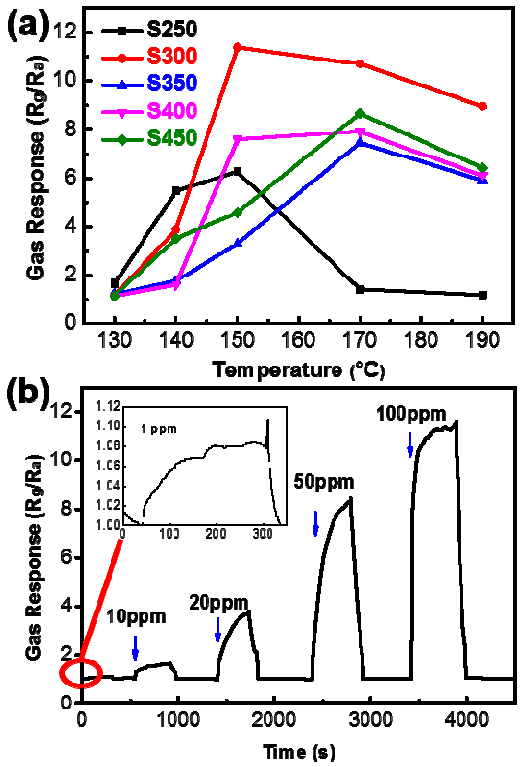

Fig. 6 (a) Gas responses of five samples as a function of different working temperatures to 100 ppm acetone concentration; (b) The response and recovery curves of S300 between different concentrations of acetone gas and air at the operating temperature of 150°C.

Further crystallographic properties information is examined via TEM. Comparing the typical TEM images shown in Fig. 4 (a)-(e), we can see that the cracked particles gradually grow up, and the size of these particles become bigger as annealing temperature increased from 250°C to 450°C, which is agree with that shown in SEM images. What's more, the differences also influence the porosity of these Co_3O_4 nanosheets, including pore volume and pore density. From HRTEM image shown in Fig. 4 (f), the lattice fringe of d=0.466 nm agrees well with the (111) crystallographic plane of the cubic Co_3O_4 phase.[27-29]

N_2 sorption measurements were evaluated for characterization of the textural properties and inner architectures of ultrathin Co_3O_4 nanosheets and gathering information about the specific surface area and pore size distribution. Fig. 5 (a) displays the nitrogen adsorption and desorption isotherms of S250–S450, all of which reveal a typical type IV adsorption isotherm with a H3-type hysteresis loop at different relative pressure ranges. Elevating the annealing temperature, the corresponding specific surface areas of samples from S250 to S450 gradually decrease, are 76.06 m^2/g, 68.73 m^2/g, 46.85 m^2/g, 21.58 m^2/g and 19.49m^2/g, respectively. The pore diameter of the samples significantly increase with the annealing temperature increasing. However, according to the Fig. 5 (b), it is obviously that the distribution of pore diameter of S300 is more intensive than others. These results indicate that the morphologies of Co_3O_4 nanosheets largely depend on the annealing temperature, and controlling the annealing conditions could regulate their microstructures.

Gas sensing properties

The gas sensing properties of the Co_3O_4 mesocrystals with different annealing temperature were studied with acetone as probe gas. The Co_3O_4 nanosheets have been uniformly coated on the Ag-Pd finger regions, which provides electrical paths between the neighbouring fingers. Firstly, the acetone sensing characteristics of the above Co_3O_4 nanosheets-based sensors were investigated for optimum operating temperature. As shown in Fig. 6 (a), the optimum operating temperatures for both S250 and S300 are 150°C, while that of S350, S400 and S450 are 170°C. Among the sensors, S300 exhibited superior sensitivity. Sensitivities of present sensors were found to increase with increasing operating temperature, attaining the maximum value (~11.4), then decrease with further increasing operating temperature. The gas adsorption and desorption kinetics on the surface of Co_3O_4 can be used to explain this behaviour. When the operating temperature is relatively low, the chemical activity of Co_3O_4 nanosheets is consequently low, leading to a low response. But if the operating temperature increases too much, some adsorbed gas molecules may escape from Co_3O_4 surfaces before reaction, because of the strong thermal motion owing to high

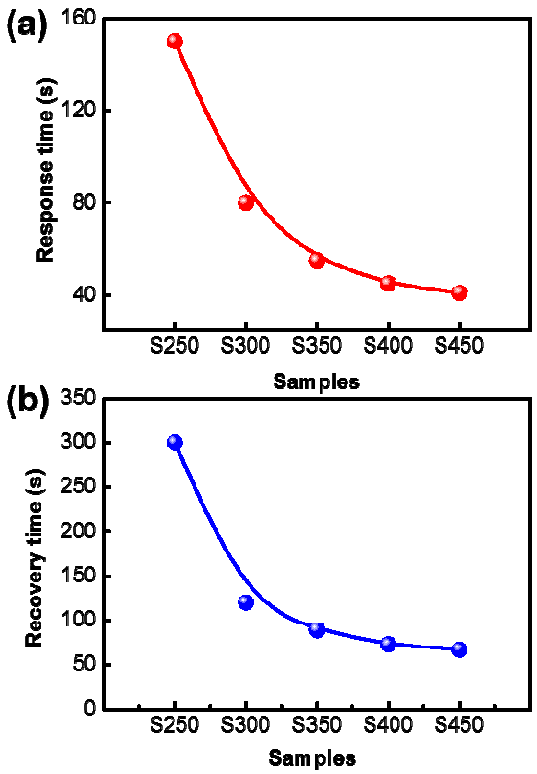

Fig. 7 (a) Response time and (b) recovery time of the samples S250-450, respectively.

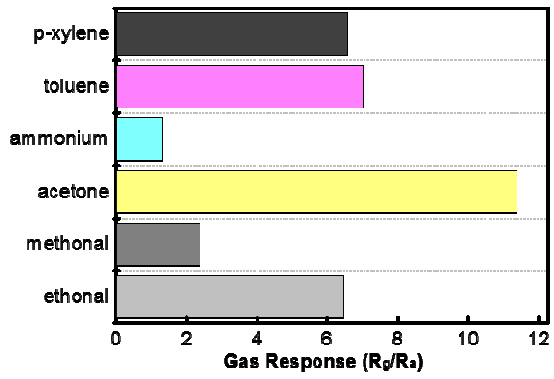

Fig. 8 The gas responses of S300 to several reducing gases with concentrations of 100 ppm at 150°C.

temperature, thus responses decrease correspondingly.[30] Therefore appropriate operating temperature is the precondition of good gas sensing property. The relation curves between the sensors response versus acetone with concentrations ranging from 1 to 100 ppm were measured at 150°C shown in Fig. 6 (b). As is reported that acetone at concentrations greater than or equal to 1.8 ppm is exhaled from diabetes patients, which is 2-6-fold higher than the 300–900 ppb of acetone exhaled by healthy people.[19] Thus, the acetone detection limit of sensor was lower than 1.8ppm is an important parameter for the applications aimed at diagnosis of diabetes. This result indicates that this kind of gas

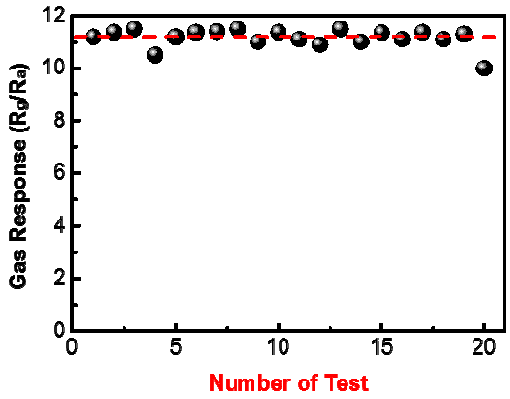

Fig. 9 The response of the Co_3O_4 sensor at 150°C to 100 ppm acetone (RH~50%) repeated with 20 times test during two months.

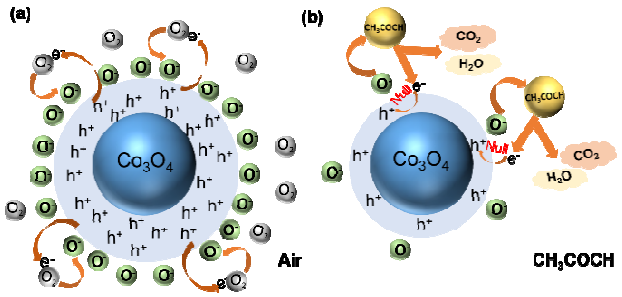

Fig.10 Schematic diagram of acetone gas sensing mechanism.

sensor can be used to analysis breath acetone for diabetes detection. With the increasing of the concentration of acetone, the response also improved rapidly. The response to 100ppm acetone gas reached ~11.4, which illustrates that the ultrathin Co_3O_4 nanosheets-based sensor not only can be used to detecting diabetes but also is useful for other fields to detect acetone with high concentration.

Another important parameter of sensor property is response-recovery time, which is calculated under 100 ppm acetone at 150°C of all samples. Fig. 7 (a) shows the response time of S250-S450, decreasing from 150 s to 41 s. And the recovery time of S250-S450 are decreased from 300 s to 65 s, shown in Fig. 7 (b).

Fig. 8 presents the acetone-selective characteristics of S300 with respect to other typical interfering gases such as ethanol, ammonium, methanol, toluene, and m-xylene with response values toward each gas at 150°C. The gas response to 100 ppm acetone vapour is significantly higher than all the other gases under the same concentration, which demonstrates that the sensors based on ultrathin porous Co_3O_4 nanosheets show high anti-interference performance that is the precondition of becoming the useful sensor to detect breath acetone for diabetes detection. The adsorption ability of ultrathin porous Co_3O_4 nanosheets to some gas molecules, such as acetone, is comparatively stronger than others, which enables it to achieve selective detection.[31-33]

To confirm the stability of samples, the response of the S300 at 150°C to 100 ppm acetone (RH~50%) repeated with 20 times test during two months. The result shown in Fig. 9 illustrates that there was almost no apparent signal attenuation during 20 times test. Therefore, we can conclude that the stability of this material

is good enough to detect acetone in a long time. However, even though this device showed good performance for acetone detecting, it does not mean that this device can be directly put into clinical use. There are lots of realistic issues should be solved firstly, such as the high humidity levels in breath, fluctuations in humidity and temperature, counteracting volatile compounds in the breath, and more.[34]

Gas sensing mechanism

The gas sensing mechanism for Co_3O_4 widely consists of the change of electrical conductivity on accounting of the chemical interaction of gas molecules with the surface involving gas adsorption, surface reaction, and desorption processes. The schematic diagram of acetone gas sensing mechanism is illustrated in Fig. 10. Herein, Co_3O_4 is a typical *p*-type semiconductor, holes are the main charge carrier. When exposed to air, the oxygen molecules adsorbed on its surface transfer to ionized oxygen species (O_2^-, O^{2-}, or O^-) by trapping electrons from Co_3O_4, forming the depletion layers. When reductive gas molecules, such as acetone, are introduced into the test chamber, these chemisorbed oxygen species will be released,[9, 35] thus, the charge carrier accumulation layer near the surface is thinned by the electrochemical interaction between O^- and gas molecules, as in the following reaction (1), which releases free electrons and neutralizes the holes in the Co_3O_4, leading to the increase of the baseline resistivity until a dynamic equilibrium condition is obtained. After the acetone flow stopped, oxygen molecules in the air are adsorbed on the surface of the sensors again, and the resistance decrease to its initial values.

$$CH_3COCH_3\ (gas) + 8O^- \rightarrow 3CO_2 + 3H_2O + 8e^- \quad (1)$$

In our experiment, we believe that the difference of sensing properties among samples with different annealing temperature is relate to the specific surface chemical composition and microstructure of these gas sensors. As TEM images shown in Fig. 4 (a)-(e), the nanoparticles in S250 and S300 are smaller than that of S350, S400 and S450, and the pore density of S300 is higher than that of S250. From Fig.5 (a), we can see the corresponding specific surface areas of S250 is slightly higher than that of S300. However, by Fig. 5 (b), it is obviously that the pore diameter of S300 is bigger than that of S250, and the distribution of pore diameter of S300 is more intensive than S250. Hence, more oxygen molecules can be adsorbed on the surface of S300 and promote the diffusion of target gases, which are the key factors for gas sensing property. Generally, the ultrathin porous structure is beneficial for gas sensing performance, allowing the gas molecules to easily penetrate and adsorb on the surface of the nanosheets and leading to fast response-recovery time as well as high sensitivity.

Conclusions

In conclusion, the gas sensor based on ultrathin porous Co_3O_4 nanosheets has been successfully synthesized through a hydrothermal technique and subsequent controlled annealing route, showing excellent performance to acetone detection at a much lower operating temperature. The response to 100 ppm acetone reached 11.4 at 150°C. What's more, the detection limit of Co_3O_4 nanosheets-based sensors is lower than 1.8 ppm that is exhaled from diabetes patients, and exhibited good reproducibility and stability. Its high-performance owes to the ultrathin structure, meso-porosity, and large specific surface area. These results indicate that the gas sensor based on ultrathin porous Co_3O_4 nanosheets is very promising for making an initial judgment of the diabetes in human beings' daily life. However, it must be raised that there are lots of problems should be overcome before put the sensor into practical use.

Notes and references

[a] *School of Materials Science and Engineering, Zhejiang University*
[b] *State Key Laboratory of Silicon Materials,*
Hangzhou 310027, People's Republic of China
E-mail: zlp1@zju.edu.cn
Tel.: + 86 571 87952625
Fax: + 86 571 87952625

1. P. Spanel and D. Smith, *Medical & Biological Engineering & Computing*, 1996, 34, 409-419.
2. P. L, R. AB and C. P, *Proc. Nat. Acad. Sci. USA*, 1971, 68, 2374-2376.
3. W. Miekisch, J. K. Schubert and G. F. Noeldge-Schomburg, *Clinica chimica acta; international journal of clinical chemistry*, 2004, 347, 25-39.
4. A. Damico, C. Dinatale, R. Paolesse, A. Macagnano, E. Martinelli, G. Pennazza, M. Santonico, M. Bernabei, C. Roscioni and G. Galluccio, *Sensors and Actuators B: Chemical*, 2008, 130, 458-465.
5. Darryl Hill and R. Binions, *International Journal on Smart Sensing and Intelligent Systems*, 2012, 5, 401-440.
6. D. Guo, D. Zhang, Naimin Li, L. Zhang and J. Yang, *IEEE Transactions on Biomedical Engineering*, 2010, 57, 2753-2763.
7. C. Ortiz-Lopez, R. Lomonaco, B. Orsak, J. Finch, Z. Chang, V. G. Kochunov, J. Hardies and K. Cusi, *Diabetes care*, 2012, 35, 873-878.
8. A. American Diabetes, J. P. Bantle, J. Wylie-Rosett, A. L. Albright, C. M. Apovian, N. G. Clark, M. J. Franz, B. J. Hoogwerf, A. H. Lichtenstein, E. Mayer-Davis, A. D. Mooradian and M. L. Wheeler, *Diabetes care*, 2008, 31 Suppl 1, S61-78.
9. J. F. Dummer, M. K. Storer, W. P. Hu, M. P. Swanney, G. J. Milne, C. M. Frampton, J. M. Scotter, G. K. Prisk and M. J. Epton, *Journal of breath research*, 2010, 4, 046001.
10. A. Kachanov, A. Charvat and F. Stoeckel, *J. Opt. Soc. Am. B*, 1995, 12, 970-979.
11. N. Makisimovich, V. Vorotyntsev, L. N. Nikitin, O. Kaskevich, P. Karabun and F. Martynenko, *Sensors and Actuators B: Chemical*, 1996, 36, 419-421.
12. M. Phillips, K. Gleeson and R. N. Cataneo, *Early Report*, 1999, 353, 1930-1933.
13. G. F. Fine, L. M. Cavanagh, A. Afonja and R. Binions, *Sensors*, 2010, 10, 5469-5502.
14. T. Akamatsu, T. Itoh, N. Izu and W. Shin, *Sensors*, 2013, 13, 12467-12481.
15. K.-I. Choi, H.-R. Kim, K.-M. Kim, D. Liu, G. Cao and J.-H. Lee, *Sensors and Actuators B: Chemical*, 2010, 146, 183-189.
16. B. Ding, M. Wang, X. Wang, J. Yu and G. Sun, *Materials Today*, 2010, 13, 16-27.
17. G. Konvalina, *Acc. Chem. Res*, 2014, 47, 66-76.
18. H. Haick, Y. Y. Broza, P. Mochalski, V. Ruzsanyi and A. Amann, *Chemical Society reviews*, 2014, 43, 1423-1449.
19. M. Righettoni and A. Tricoli, *Journal of breath research*, 2011, 5, 037109.
20. L. Liu, S. Li, J. Zhuang, L. Wang, J. Zhang, H. Li, Z. Liu, Y. Han, X. Jiang and P. Zhang, *Sensors and Actuators B: Chemical*, 2011, 155, 782-788.
21. P. Song, Q. Wang and Z. Yang, *Sensors and Actuators B: Chemical*, 2012, 173, 839-846.

22. X. Zhou, W. Feng, C. Wang, X. Hu, X. Li, P. Sun, K. Shimanoe, N. Yamazoe and G. Lu, *J. Mater. Chem. A*, 2014, 2, 17683-17690.
23. Z. Wen, L. Zhu, W. Mei, L. Hu, Y. Li, L. Sun, H. Cai and Z. Ye, *Sensors and Actuators B: Chemical*, 2013, 186, 172-179.
24. Z. Wen, L. Zhu, W. Mei, Y. Li, L. Hu, L. Sun, W. Wan and Z. Ye, *Journal of Materials Chemistry A*, 2013, 1, 7511.
25. Z. Wen, L. Zhu, Y. Li, Z. Zhang and Z. Ye, *Sensors and Actuators B: Chemical*, 2014, 203, 873-879.
26. Z. Wen, L. Zhu, Z. Zhang and Z. Ye, *Sensors and Actuators B: Chemical*, 2015, 208, 112-121.
27. X. Xiao, X. Liu, H. Zhao, D. Chen, F. Liu, J. Xiang, Z. Hu and Y. Li, *Advanced materials*, 2012, 24, 5762-5766.
28. X. Liu, J. Zhang, S. Wu, D. Yang, P. Liu, H. Zhang, S. Wang, X. Yao, G. Zhu and H. Zhao, *RSC Advances*, 2012, 2, 6178.
29. Y. Teng, L. X. Song, L. B. Wang and J. Xia, *The Journal of Physical Chemistry C*, 2014, 118, 4767-4773.
30. S. Wang, C. Xiao, P. Wang, Z. Li, B. Xiao, R. Zhao, T. Yang and M. Zhang, *Materials Letters*, 2014, 137, 289-292.
31. L. Li, S. He, M. Liu, C. Zhang and W. Chen, *Analytical chemistry*, 2015, 87, 1638-1645.
32. M. Hakim, Y. Y. Broza, O. Barash, N. Peled, M. Phillips, A. Amann and H. Haick, *Chemical reviews*, 2012, 112, 5949-5966.
33. B. Wang, J. C. Cancilla, J. S. Torrecilla and H. Haick, *Nano letters*, 2014, 14, 933-938.
34. G. Konvalina and H. Haick, *ACS applied materials & interfaces*, 2012, 4, 317-325.
35. L. Qin, J. Xu, X. Dong, Q. Pan, Z. Cheng, Q. Xiang and F. Li, *Nanotechnology*, 2008, 19, 185705.